Chapter 4

Multiple-IRS Aided Wireless Networks Over Nakagami-m Fading Channels

In this Chapter, the OP for wireless systems aided by multiple IRS panels operating over Nakagami-m fading channels is analyzed. Two closed-form expressions for OP utilizing the CLT and LSE are derived. Moreover, a novel asymptotic OP expression is developed, leading to the identification of a unique diversity order.

4.1 Introduction

IRS-assisted systems have garnered substantial attention in the recent years from both academia and industry for the next generation wireless networks [93–95]. An IRS comprises of a planar array of electromagnetic elements capable of precisely manipulating incident electromagnetic waves. These surfaces are ingeniously designed

to exert control over propagation of radio waves, thereby offering the potential to revolutionize wireless communication by enhancing signal quality, reducing interference, and optimizing network performance. Closely related IRS-assisted works in literature are summarised below.

4.1.1 Related Works

Several recent research studies have explored the performance of IRS over fading channels due to their promising characteristics [15, 26, 32–36, 40, 72, 96–108]. A mathematical framework for the calculation of the ABER performance of IRS-assisted SISO systems is provided for Rayleigh fading channels in [32]. In [33], authors assess OP in a SISO wireless communication system with multi-IRS over Rician fading channels, emphasizing IRS panel selection, offering closed-form expressions for OP. In [15], authors have proposed a transmission scheme for downlink multi-IRS assisted NOMA systems with the consideration of second-order reflection and Rician fading channels. Authors in [34] study the feasibility and benefits of a multi-IRS dual-hop decode-and-forward (DF) relaying system in Nakagami-m fading channels to improve ergodic rate performance. In [26], authors explore the effectiveness of IRS in wireless networks operating on Rician fading channels. They derive precise closed-form approximations for different performance metrics, including OP, ABER, and channel capacity. Ergodic capacity and OP analysis of SISO communication systems aided by IRS, considering the direct link between the transmitter and receiver in Rician fading are given in [35]. In [36], Bhagat et al. derive closed-form expressions for ABER for both coherent Gray-coded rectangular quadrature amplitude modulation (RQAM) and non-coherent modulation schemes for IRS-aided SISO systems in Hoyt faded channels. Authors in [96] obtain closed-form expressions for the secrecy OP and strictly positive secrecy capacity probability for four

combinations of eavesdropping scenarios and relay modes and also provide corresponding asymptotic solutions. In [97], the performance of active IRS in a single-cell wireless network is investigated, proposing a customized deployment strategy and highlighting the importance of selecting the right density of active IRS elements to achieve improved system performance and higher spatial throughput compared to passive IRS deployment in specific scenarios. Authors in [40] examine the uplink OP of NOMA with IRS assistance in scenarios where users have both direct and reflection links. In [98], Charishma et al. investigate the OP of an IRS assisted communication system in a κ-μ fading environment, considering phase errors due to quantization at the IRS and offers both an exact expression and three accurate approximations for the outage probability, with a focus on quantization bits, IRS placement, and number of elements, while demonstrating their effectiveness through Monte Carlo simulations.. In [99], authors evaluate the security of device-to-device (D2D) communication in cellular networks with an IRS, offering closed-form expressions for secrecy OP, introducing a secrecy spectrum allocation problem, and showing that more IRS elements improve security.. In [100], the outage performance of uplink IRS-assisted NOMA/OMA networks in a two-user equipment is investigated, considering both direct and reflected links, and closed-form OP expressions are derived. Authors in [101] investigate outage performance in an IRS-assisted mobile edge computing network, proposes IRS unit selection criteria, develop analytical expressions, and optimize IRS deployment for improved system performance. In [102], authors introduce a deep reinforcement learning approach for optimizing a centralized IRS-assisted NOMA-beam-forming (BF) system in wireless networks, enhancing capacity and energy efficiency while addressing channel uncertainties and mitigating interference, resulting in improved performance with reduced complexity. In [103], authors evaluate the performance of a cascaded IRS network with imperfect phase estimation, providing closed-form expressions for OP, ergodic capacity, and

ABER. Authors in [72] explore a network with multi-IRS and analyze the selection of the RIS with the highest SNR, examining OP and sum-rate. In [104], authors introduce randomly reconfigurable surfaces (RRSs) designed to diffuse incoming waves and assess the performance of an RRS-assisted communication network, providing closed-form expressions for various performance metrics and considering scenarios where links undergo different fading types. In [105], authors explore communication through a large IRS with phase errors, treating the composite channel as having Nakagami scalar fading, and show that the system remains robust against phase errors, even with a limited number of reflectors. In [106], Ni et al. investigate an IRS-assisted D2D communication system in Nakagami-m fading, analyzing OP, diversity order, ergodic rates, and energy efficiency improvements, highlighting the benefit of optimal phase shifts and proximity of the IRS to D2D devices for enhanced performance. Authors in[107] assess the performance of an uplink MISO IRS-based system, finding that using MRC with optimal phase-shift configuration yields the best performance, and selection-combining with optimal phase-shift can outperform MRC when the number of antenna settings is limited, supported by Monte-Carlo simulations. In [108], authors investigate integrating IRS into wireless vehicular networks, introduce partial IRS selection to improve capacity and reduce errors, provide analytical expressions for performance metrics, compare it to partial relaying, and excel in terms of security and performance. All related works are summarized in Table 4.1.

To the best of the our' knowledge, no prior work has analyzed multiple IRS-assisted SISO systems with IRS panel selection in the context of generalized non-identically distributed Nakagami-m fading channels. Therefore, it is both useful and intriguing to analyze the system's performance when multiple IRS (MIRS) are deployed to enhance overall system performance.

TABLE 4.1: A summary of related works

Ref.	**Performance Metrics**	**System Model**	**Fading Model**
[32]	ABER	IRS+SISO	Rayleigh
[33]	OP	Multi-IRS+SISO	Rician
[15]	Joint transmit power and phase shift optimization	IRS+NOMA	Rician
[34]	Ergodic Rate	Multi-IRS+DF	Nakagami-m
[26]	OP, ABER, Channel Capacity	IRS+SISO	Rician
[35]	Ergodic capacity, OP	IRS+SISO	Rician
[36]	ABER	IRS+SISO	Hoyt
[96]	Secrecy OP	IRS + VLC/RF	Rayleigh
[97]	Average SNR, deployment strategy	Active IRS	Nakagami-m
[40]	OP	Uplinnk NOMA +IRS	Nakagami-m
[98]	OP	IRS+ Phase errors	κ-μ
[99]	Secrecy OP	IRS +D2D	Rayleigh
[100]	OP	IRS+NOMA/OMA	Nakagami-m
[101]	OP	IRS +mobile edge computing network	Rayleigh
[102]	OP, Energy efficiency	IRS+NOMA-BF	Rician/Nakagami-m
[103]	OP, ergodic capacity, ABER	Cascaded-IRS	Nakagami-m
[72]	OP, sum-rate	Multi-IRS+ Selection of best IRS	Rayleigh
[104]	OP, ergodic capacity, ABER	RRS+SISO	Nakagami-m
[105]	ABER	Large IRS+SISO	Nakagami-m
[106]	OP, diversity order, ergodic rates	IRS+ D2D communication	Nakagami-m
[107]	OP	IRS+MISO	Rayleigh
[108]	ABER, ergodic capacity	IRS+ vehicular networks	Rayleigh

Contributions: In this chapter, we explore IRS panel selection for SISO systems, enhancing channels for improved performance. The MIRS panels-assisted systems

allow adjusting phase shifts after panel selection, valuable in cost-constrained scenarios. We consider the Nakagami-m fading channel, which is a versatile fading model for practical wireless channels. Our main contributions in this context are as follows:

- We obtain two approximate expressions for the OP of MIRS by employing the CLT and the LSE techniques, respectively. Our analysis encompasses the challenges posed by independent and non-identically distributed (i.n.d) Nakagami-m fading channels.
- We also derive a new generalized asymptotic OP expression and employ it to obtain the diversity order expression
- We thoroughly analyze the impact of various system parameters, including the fading parameter and the number of IRS panels.

The subsequent sections of this chapter are structured as follows: Section 4.2 provides the system and channel models. Section 4.3 presents both approximate and asymptotic OP derivations. Section 4.4 delves into the discussion of numerical and simulation results. Section 4.5 offers a summary of the chapter's findings and their consequential implications.

4.2 System and Channel Models

A SISO communication system assisted with L IRS panels is considered, as shown in Figure 4.1. These L IRS panels are deployed between the Tx and Rx to enhance the system's performance. Each panel has N_l $(1 \leq l \leq L)$ reflecting elements and the CSI is available at IRS panels [93, 109]. The receiver will receive signals from all the

IRS panels at different time instants with the help of the desired delay introduced at each IRS panel. Then the receiver will compare the SNR of all the received signals and choose the best-received signal that has the highest SNR for further processing and decoding. We make the assumption that Nakagami-m fading characterizes each individual link. Additionally, it is assumed that the direct path between the Tx and the Rx is completely blocked due to severe fading [15, 35, 109]. This presented system model can be used as the uplink of next-generation wireless communication systems to improve the quality of service and enhance the cellular user experience.

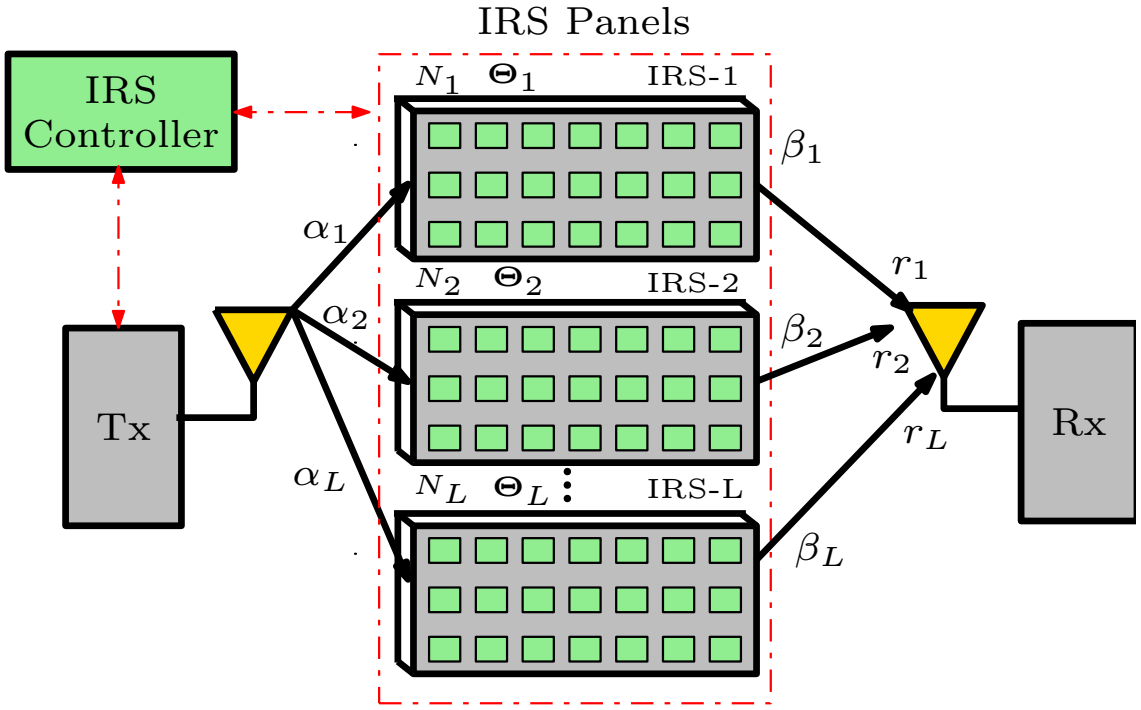

FIGURE 4.1: Multiple IRS-aided SISO wireless network with IRS panel selection.

The received signal coming from the l-th IRS panel can be written as [32]

$$r_l = \sqrt{P}\left(\boldsymbol{\beta_l}^T \boldsymbol{\Theta_l} \boldsymbol{\alpha_l}\right) x_t + n_l, \qquad 1 \leq l \leq L, \tag{4.1}$$

where x_t represents the transmitted message signal with unit energy and P denotes the transmit power. The vectors $\boldsymbol{\alpha}_l = [\alpha_{l1}, \alpha_{l2}, \ldots \alpha_{lN_l}]$ and $\boldsymbol{\beta}_l = [\beta_{l1}, \beta_{l2}, \ldots, \beta_{lN_l}]$

represent the Nakagami-m channel coefficients between the Tx and the lth IRS panel, and between the lth IRS panel and the Rx, respectively. Represented as $\mathbf{\Theta}_l = \text{diag}\{[e^{j\theta_{l1}}, e^{j\theta_{l2}}, \ldots, e^{j\theta_{lN_l}}]\}$, this diagonal matrix encapsulates the dynamic phase modulation introduced by the reflecting meta-surfaces of the l^{th} IRS panel [15, 32, 93, 109]. d_{α_l} and δ_{α_l} represent the distance, and the path loss exponent between the Tx and the l^{th} IRS panel, respectively. Similarly, d_{β_l} and δ_{β_l} are the distance and path loss exponent between the lth IRS panel and the Rx. n_l is the additive white Gaussian noise having variance N_0 and zero mean at the Rx node. The expression for the PDF of a Nakagami-m distributed random variable (RV) $Y \in \{|\alpha_{li}|, |\beta_{li}|, 1 \leq i \leq N_l, 1, 1 \leq l \leq L\}$ can be written as [8]

$$f_Y(y) = \frac{2m_y^{m_y} y^{2m_y-1}}{\Gamma(m_y)\Omega_y^{m_y}} \exp\left(-\frac{m_y}{\Omega_y} y^2\right), \tag{4.2}$$

where $\Gamma(\cdot)$ is the Gamma function, $\Omega_y = \mathbb{E}[Y^2]$ is the average power, $\mathbb{E}[\cdot]$ denotes expectation operator, and m_y is the fading parameter. With the aid of [77, (8.310.1)], the nth moment of RV Y can be obtained as

$$\mathbb{E}[Y^n] = \int_0^\infty y^n f_Y(y) dy = \left(\frac{\Omega_y}{m_y}\right)^{0.5n} \frac{\Gamma(m_y + 0.5n)}{\Gamma(m_y)}. \tag{4.3}$$

We have assumed that the perfect CSI and the phase information is available at each IRS panel [32, 93]. Hence, after multiplying the optimal co-phasing matrix $\mathbf{\Theta}_l$, the instantaneous optimal SNR γ_l of l-th received signal from l^{th} panel can be expressed as [32]

$$\gamma_l = \gamma_0 \left(\sum_{i=1}^{N_l} |\alpha_{li}| \, |\beta_{li}|\right)^2, \tag{4.4}$$

where $\gamma_0 = \frac{P}{N_0}$ is the transmit SNR. Since the receiver will process the highest SNR signal received from the best-selected IRS panel. Thus, the output SNR γ_{sc} at the

output of the receiver can be written as [8]

$$\gamma_{sc} = \max_{1 \leq l \leq L} \{\gamma_l\} . \tag{4.5}$$

4.3 Analysis of Outage Probability

The OP for the selected SISO communication system, employing the best IRS panel selection, can be represented as [8]

$$P_{\text{out}} = \Pr\left(\gamma_{sc} \leq \gamma_{th}\right) = \prod_{l=1}^{L} F_{\gamma_l}\left(\gamma_{th}\right), \tag{4.6}$$

where $\Pr(\cdot)$ denotes probability operator, $F_{\gamma_l}(\cdot)$ is the cumulative distribution function (CDF) of instantaneous SNR γ_l, and γ_{th} represents the predefined threshold SNR. In order to calculate the OP, an expression for $F_{\gamma_l}(\cdot)$ needs to be derived.

4.3.1 Approximate OP Expression

The instantaneous SNR at the Rx node due to the l^{th} IRS panel can be re-expressed as $\gamma_l = \mathcal{B}_l^2 \gamma_0$, where $\mathcal{B}_l = \sum_{i=1}^{N_l} \mathcal{B}_{li}$ and $\mathcal{B}_{li} = |\alpha_{li}|\,|\beta_{li}|$. As we know that $|\alpha_{li}|$ and $|\beta_{li}|$ are independent Nakagami-m distributed RVs. For simplicity, we assume that for fixed l, $|\alpha_{li}|$ and $|\beta_{li}|$ are Nakagami-m distributed RVs with parameters $(m_{\alpha_l}, \Omega_{\alpha_l})$ and $(m_{\beta_l}, \Omega_{\beta_l})$, respectively. Hence, using (4.3), the mean and the square of the standard deviation of RV $\mathcal{B}_{li}$ can be given as $\mu_{\mathcal{B}_{li}} = \mathbb{E}[\mathcal{B}_{li}] = \mathbb{E}[|\alpha_{li}|]\mathbb{E}[|\beta_{li}|]$, and $\sigma^2_{\mathcal{B}_{li}} = \mathbb{E}[\mathcal{B}_{li}^2] - (\mathbb{E}[\mathcal{B}_{li}])^2 = \mathbb{E}[|\alpha_{li}|^2]\mathbb{E}[|\beta_{li}|^2] - (\mathbb{E}[|\alpha_{li}|]\mathbb{E}[|\beta_{li}|])^2$, respectively. Note that $\mathbb{E}[|\alpha_{li}|]$ and $\mathbb{E}[|\beta_{li}|]$ can be obtained by putting $n = 1$ into (4.3) and $\mathbb{E}[|\alpha_{li}|2]$ and $\mathbb{E}[|\beta_{li}|^2]$ can be also got by putting $n = 2$ into (4.3).

4.3.1.1 CLT Aproach

Obtaining a precise and analytically manageable expression for $F_{\gamma_l}(\cdot)$ is not a feasible endeavor. However, when the number of reflecting surfaces N_l, is sufficiently large (i.e., $N_l >> 1$), the central limit theorem can be employed. This allows modeling the random variable $\mathcal{B}_l$ as a normally distributed random variable with variance $\sigma^2_{\mathcal{B}_l} = N_l\sigma^2_{\mathcal{B}_{li}}$ and mean $\mu_{\mathcal{B}_l} = N_l\mu_{\mathcal{B}_{li}}$ [35]. Hence, the PDF of $\mathcal{B}_l$ can be given by [9] $f_{\mathcal{B}_l}(x) = \frac{\Delta_{\mathcal{B}_l}}{\sqrt{2\pi\sigma^2_{\mathcal{B}_l}}} \exp\left(-\frac{\left(x-\mu_{\mathcal{B}_l}\right)^2}{2\sigma^2_{\mathcal{B}_l}}\right)$, where $\Delta_{\mathcal{B}_l} = \left(0.5 + 0.5\text{erf}\left(\sqrt{\frac{\mu^2_{\mathcal{B}_l}}{2\sigma^2_{\mathcal{B}_l}}}\right)\right)^{-1}$ and $\text{erf}(\cdot)$ is the error function [9]. The corresponding CDF of $\mathcal{B}_l$ is expressed as

$$F_{\mathcal{B}_l}(x) = \int_{-\infty}^{x} f_{\mathcal{B}_l}(t)dt = 1 - \Delta_{\mathcal{B}_l} Q\left(\frac{x-\mu_{\mathcal{B}_l}}{\sigma_{\mathcal{B}_l}}\right), \tag{4.7}$$

where $Q(\cdot)$ denotes the Gaussian Q-function [9]. Now, one can get the CDF of γ_l as the following

$$F_{\gamma_l}(x) = \Pr(\gamma_l \leq x) = 1 - \Delta_{\mathcal{B}_l} Q\left(\frac{\sqrt{\frac{x}{\gamma_0}} - \mu_{\mathcal{B}_l}}{\sigma_{\mathcal{B}_l}}\right). \tag{4.8}$$

4.3.1.2 LSE Approach

It can provide good approximations for a small number of IRS elements, unlike the CLT (as observed in Figure 4.2). The first-term expansion of $\mathcal{B}_l$ within the framework of the LSE offers a highly accurate approximation of its PDF as [26]

$$f_{\mathcal{B}_l}(x) = \frac{x^{\tau_l} \exp\left(-\frac{x}{\eta_l}\right)}{\eta_l^{\tau_l+1}\Gamma(\tau_l+1)}, \tag{4.9}$$

where $\tau_l = \frac{\mu^2_{\mathcal{B}_l}}{\sigma^2_{\mathcal{B}_l}} - 1$ and $\eta_l = \frac{\sigma^2_{\mathcal{B}_l}}{\mu_{\mathcal{B}_l}}$. The CDF expression of $\mathcal{B}_l$ can be written as

$$F_{\mathcal{B}_l}(x) = \int_0^x f_{\mathcal{B}_l}(t)dt = \frac{\Upsilon\left(\tau_l + 1, \frac{x}{\eta_l}\right)}{\Gamma\left(\tau_l + 1\right)}, \tag{4.10}$$

where the lower incomplete gamma function $\Upsilon\left(\cdot,\cdot\right)$ is referenced from [77, (8.350.1)]. We can now derive the CDF for γ_l as follows:

$$F_{\gamma_l}(x) = \Pr\left(\gamma_l \leq x\right) = \frac{\Upsilon\left(\tau_l + 1, \frac{\sqrt{\frac{x}{\gamma_0}}}{\eta_l}\right)}{\Gamma\left(\tau_l + 1\right)}. \tag{4.11}$$

By substituting either (4.8) or (4.11) into (4.6), we can obtain two approximate OP for the SISO wireless system under consideration, i.e.,

$$P_{\text{out}} = \begin{cases} \prod_{l=1}^{L}\left(1 - \Delta_{\mathcal{B}_l} Q\left(\frac{\sqrt{\frac{\gamma_{th}}{\gamma_0}} - \mu_{\mathcal{B}_l}}{\sigma_{\mathcal{B}_l}}\right)\right), & \text{CLT} \\ \\ \prod_{l=1}^{L} \frac{\Upsilon\left(\tau_l+1, \frac{\sqrt{\frac{\gamma_{th}}{\gamma_0}}}{\eta_l}\right)}{\Gamma(\tau_l+1)}, & \text{LSE} \end{cases} \tag{4.12}$$

4.3.2 Asymptotic OP Expression

Asymptotic OP provides valuable insights into the channel fading conditions of a communication system in a very high SNR scenario. In the asymptotic analysis, we make the assumption that $\gamma_0 \to \infty$ or $\Omega_y \to \infty$. The asymptotic OP into two different fading conditions is derived next.

4.3.2.1 Non-Identical Fading Conditions

We assume that the fading conditions are non-identical nature. For ease of representation, the PDF of RV $Y \in \{|\alpha_{li}|, |\beta_{li}|, 1 \leq i \leq N_l, 1 \leq l \leq L\}$ is re-expressed as

$$f_Y(y) = \eta_y y^{2m_y-1} \exp\left(-\lambda_y y^2\right), \tag{4.13}$$

where $\eta_y = \frac{2m_y^{m_y}}{\Gamma(m_y)\Omega_y^{m_y}}$ and $\lambda_y = \frac{m_y}{\Omega_y}$. Now, assuming $m_{\alpha_{li}} > m_{\beta_{li}}$ and using [79, (2.3.16.1)], the PDF expression of $\mathcal{B}_{li}$ can be obtain as

$$\begin{aligned} f_{\mathcal{B}_{li}}(b_{li}) &= \int_0^\infty \frac{1}{\alpha_{li}} f_{|\alpha_{li}|}(\alpha_{li}) f_{|\beta_{li}|}\left(\frac{b_{li}}{\alpha_{li}}\right) d\alpha_{li} \\ &= \eta_{\alpha_{li}}\eta_{\beta_{li}} \left(\frac{\lambda_{\beta_{li}}}{\lambda_{\alpha_{li}}}\right)^{\frac{m_{\alpha_{li}}-m_{\beta_{li}}}{2}} b_{li}^{m_{\alpha_{li}}+m_{\beta_{li}}-1} \\ &\times K_{m_{\alpha_{li}}-m_{\beta_{li}}}\left(2b_{li}\sqrt{\lambda_{\alpha_{li}}\lambda_{\beta_{li}}}\right), \quad m_{\alpha_{li}} > m_{\beta_{li}} \end{aligned} \tag{4.14}$$

For a small argument of the modified generalized order second-kind Bessel function $K_v(\cdot)$, a notable relationship can be established, as documented in [75, (9.6.9)]. This relationship is given by $\lim_{x\to 0} K_v(x) \approx \frac{1}{2}\Gamma(v)\left(\frac{1}{2}x\right)^{-v}$, $Re(v) > 0$. Leveraging this approximation, we can derive an asymptotic PDF of $\mathcal{B}_{li}$ as

$$f^{\infty}_{\mathcal{B}_{li}}(b_{li}) \approx \mathcal{C}_{li}\, b_{li}^{2m_{\beta_{li}}-1}, \qquad m_{\alpha_{li}} > m_{\beta_{li}} \tag{4.15}$$

where $\mathcal{C}_{li} = \frac{\eta_{\alpha_{li}}\eta_{\beta_{li}}}{2\lambda_{\alpha_{li}}^{m_{\alpha_{li}}-m_{\beta_{li}}}}\Gamma\left(m_{\alpha_{li}} - m_{\beta_{li}}\right)$. Furthermore, for $m_{\beta_{li}} > m_{\alpha_{li}}$ case, one can also get asymptotic PDF of $\mathcal{B}_{li}$ as

$$f^{\infty}_{\mathcal{B}_{li}}(b_{li}) \approx \mathcal{D}_{li}\, b_{li}^{2m_{\alpha_{li}}-1}, \qquad m_{\beta_{li}} > m_{\alpha_{li}} \tag{4.16}$$

where $\mathcal{D}_{li} = \frac{\eta_{\alpha_{li}}\eta_{\beta_{li}}}{2\lambda_{\beta_{li}}^{m_{\beta_{li}}-m_{\alpha_{li}}}}\Gamma\left(m_{\beta_{li}} - m_{\alpha_{li}}\right)$. Now, combing (4.15) and (4.16), we can write the following

$$f_{\mathcal{B}_{li}}(b_{li}) \approx \Lambda_{li}\, b_{li}^{2\min\{m_{\alpha_{li}},m_{\beta_{li}}\}-1}, \qquad m_{\alpha_{li}} \neq m_{\beta_{li}} \tag{4.17}$$

where $\Lambda_{li} \in \{\mathcal{C}_{li}, \mathcal{D}_{li}\}$. Hence, we can express the asymptotic MGF of $\mathcal{B}_{li}$ as

$$\mathcal{M}_{\mathcal{B}_{li}}^{\infty}(s) = \mathcal{L}\left\{f_{\mathcal{B}_{li}}^{\infty}(b_{li})\right\} \approx \mathcal{E}_{li}\, s^{-2\min\{m_{\alpha_{li}},m_{\beta_{li}}\}}, \tag{4.18}$$

where $\mathcal{L}\{\cdot\}$ and s denote the Laplace transform operator and variable, respectively, $\mathcal{E}_{li} = \Lambda_{li}\Gamma\left(2\min\{m_{\alpha_{li}}, m_{\beta_{li}}\}\right)$. Since $\mathcal{B}_{li}$s are independent random variables, the expression for the asymptotic MGF of $\mathcal{B}_l$ is as follows.

$$\mathcal{M}_{\mathcal{B}_l}^{\infty}(s) = \prod_{i=1}^{N_l}\mathcal{M}_{\mathcal{B}_{li}}^{\infty}(s) \approx \left(\prod_{i=1}^{N_l}\mathcal{E}_{li}\right) s^{-2\sum_{i=1}^{N_l}\min\{m_{\alpha_{li}},m_{\beta_{li}}\}}. \tag{4.19}$$

By performing the inverse Laplace transform on (4.19), we can derive the asymptotic PDF expression for $\mathcal{B}_l$ as

$$\begin{aligned} f_{\mathcal{B}_l}^{\infty}(b_l) &= \mathcal{L}^{-1}\left\{\mathcal{M}_{\mathcal{B}_l}^{\infty}(s)\right\} \\ &\approx \frac{\left(\prod_{i=1}^{N_l}\mathcal{E}_{li}\right) b_l^{2\sum_{i=1}^{N_l}\min\{m_{\alpha_{li}},m_{\beta_{li}}\}-1}}{\Gamma\left(2\sum_{i=1}^{N_l}\min\{m_{\alpha_{li}}, m_{\beta_{li}}\}\right)}. \end{aligned} \tag{4.20}$$

Further, using the transformation of RV, the asymptotic PDF expression of γ_l is given as

$$f_{\gamma_l}^{\infty}(\gamma_l) \approx \frac{\left(\prod_{i=1}^{N_l}\mathcal{E}_{li}\right)(\gamma_l/\gamma_0)^{\sum_{i=1}^{N_l}\min\{m_{\alpha_{li}},m_{\beta_{li}}\}-1}}{2\Gamma\left(2\sum_{i=1}^{N_l}\min\{m_{\alpha_{li}}, m_{\beta_{li}}\}\right)\gamma_0}. \tag{4.21}$$

By applying the Laplace transform to (4.21), we can derive the asymptotic MGF expression for γ_l as

$$\mathcal{M}_{\gamma_l}^{\infty}(s) = \mathcal{L}\left\{f_{\gamma_l}^{\infty}(\gamma_l)\right\} \approx \frac{\Gamma\left(\sum_{i=1}^{N_l} \min\{m_{\alpha_{li}}, m_{\beta_{li}}\}\right)}{2\Gamma\left(2\sum_{i=1}^{N_l} \min\{m_{\alpha_{li}}, m_{\beta_{li}}\}\right)} \times \frac{\left(\prod_{i=1}^{N_l} \mathcal{E}_{li}\right) s^{-\sum_{i=1}^{N_l} \min\{m_{\alpha_{li}}, m_{\beta_{li}}\}}}{\gamma_0^{\sum_{i=1}^{N_l} \min\{m_{\alpha_{li}}, m_{\beta_{li}}\}}}. \tag{4.22}$$

Hence, the CDF expression of RV γ can be obtained as

$$F_{\gamma_l}^{\infty}(\gamma_l) = \mathcal{L}^{-1}\left\{\frac{\mathcal{M}_{\gamma_l}^{\infty}(s)}{s}\right\} \approx \left(\mathcal{G}_l \frac{\gamma_l^{\sum_{i=1}^{N_l} \min\{m_{\alpha_{li}}, m_{\beta_{li}}\}}}{\gamma_0^{\sum_{i=1}^{N_l} \min\{m_{\alpha_{li}}, m_{\beta_{li}}\}}}\right), \tag{4.23}$$

where $\mathcal{G}_l = \left(\prod_{i=1}^{N_l} \mathcal{E}_{li}\right) / \Gamma\left(2\sum_{i=1}^{N_l} \min\{m_{\alpha_{li}}, m_{\beta_{li}}\} + 1\right)$.

4.3.2.2 Identical Fading Conditions

For identical fading conditions, the PDF of RV $Y \in \{|\alpha_{li}|, |\beta_{li}|, 1 \leq i \leq N_l, 1 \leq l \leq L\}$ is re-written as

$$f_Y(y) = \eta y^{2m-1} \exp\left(-\lambda y^2\right), \tag{4.24}$$

where $\eta = \frac{2m^m}{\Gamma(m)\Omega^m}$ and $\lambda = \frac{m}{\Omega}$. Now, using [79, (2.3.16.1)],

the PDF expression of $\mathcal{B}_{li}$ can be obtain as

$$\begin{aligned} f_{\mathcal{B}_{li}}(b_{li}) &= \int_0^{\infty} \frac{1}{\alpha_{li}} f_{|\alpha_{li}|}(\alpha_{li})\, f_{|\beta_{li}|}\left(\frac{b_{li}}{\alpha_{li}}\right) d\alpha_{li} \\ &= \eta^2\, b_{li}^{2m-1}\, K_0\left(2b_{li}\lambda\right), \qquad m_{\alpha_{li}} = m_{\beta_{li}} = m. \end{aligned} \tag{4.25}$$

For a small argument of the modified zero-order second kind Bessel function $K_0(\cdot)$, a relevant relation can be found in [75, (9.6.8)], which states that $\lim_{x\to 0} K_0(x) \approx -\ln x$[1]. Leveraging this relationship, we can approximate the asymptotic PDF expression of $\mathcal{B}_{li}$ as

$$f^{\infty}_{\mathcal{B}_{li}}(b_{li}) \approx \theta\, \eta^2\, b_{li}^{2m-1}; \qquad b_{li} \geq 0 \tag{4.26}$$

where θ is defined as the limit of $-\ln(2\lambda)$ as Ω approaches infinity, with $\ln(\cdot)$ representing the natural logarithm. Consequently, we can express the asymptotic MGF of $\mathcal{B}_{li}$ as follows:

$$\mathcal{M}^{\infty}_{\mathcal{B}_{li}}(s) = \mathcal{L}\left\{f^{\infty}_{\mathcal{B}_{li}}(b_{li})\right\} \approx \theta\, \eta^2\, \Gamma(2m)\; s^{-2m}. \tag{4.27}$$

Since $\mathcal{B}_{li}$s are independent and identically random variables, we can represent the asymptotic MGF of $\mathcal{B}_l$ as

$$\mathcal{M}^{\infty}_{\mathcal{B}_l}(s) = \prod_{i=1}^{N_l} \mathcal{M}^{\infty}_{\mathcal{B}_{li}}(s) \approx \mathcal{U}_l\, s^{-2mN_l}, \tag{4.28}$$

where $\mathcal{U}_l = \left(\theta\, \eta^2\, \Gamma(2m)\right)^{N_l}$. Applying the inverse Laplace transform to (4.28) yields the asymptotic PDF expression for $\mathcal{B}_l$ as

$$f^{\infty}_{\mathcal{B}_l}(b_l) = \mathcal{L}^{-1}\left\{\mathcal{M}^{\infty}_{\mathcal{B}_l}(s)\right\} \approx \frac{\mathcal{U}_l b_l^{2mN_l-1}}{\Gamma(2mN_l)}. \tag{4.29}$$

By applying an RV transformation, we derive the asymptotic PDF expression for γ_l as

$$f^{\infty}_{\gamma_l}(\gamma_l) \approx \frac{\mathcal{U}_l \gamma_l^{mN_l-1}}{2\Gamma(2mN_l)\gamma_0^{mN_l}}. \tag{4.30}$$

[1]Note that, in this approximation, we have omitted the $-\ln b_{li}$ term.

Utilizing the Laplace transform on (4.30), we can derive the asymptotic MGF expression for γ as

$$\mathcal{M}_{\gamma_l}^{\infty}(s) = \mathcal{L}\left\{f_{\gamma_l}^{\infty}(\gamma_l)\right\} \approx \frac{\mathcal{U}_l \Gamma\left(mN_l\right)}{2\Gamma(2mN_l)\gamma_0^{mN_l} s^{mN_l}}. \tag{4.31}$$

Hence, the CDF expression of RV γ_l can be obtained as

$$F_{\gamma_l}^{\infty}(\gamma_l) = \mathcal{L}^{-1}\left\{\frac{\mathcal{M}_{\gamma_l}^{\infty}(s)}{s}\right\} \approx \frac{\mathcal{U}_l \gamma_l^{mN_l}}{\Gamma(2mN_l+1)\gamma_0^{mN_l}}. \tag{4.32}$$

Using (4.23) and (4.32) into (4.6), the asymptotic OP of the proposed SISO wireless system assisted by MIRS panels can be written as

$$P_{\text{out}}^{\infty} = \begin{cases} \prod_{l=1}^{L}\left(\mathcal{G}_l \frac{\gamma_{th}^{\left(\sum_{i=1}^{N_l}\min\{m_{\alpha_{li}}, m_{\beta_{li}}\}\right)}}{\gamma_0^{\left(\sum_{i=1}^{N_l}\min\{m_{\alpha_{li}}, m_{\beta_{li}}\}\right)}}\right); \ m_{\alpha_{li}} \neq m_{\beta_{li}} \\ \\ \prod_{l=1}^{L}\left(\frac{\mathcal{U}_l \gamma_{th}^{mN_l}}{\Gamma(2mN_l+1)\gamma_0^{mN_l}}\right); \ m_{\alpha_{li}} = m_{\beta_{li}} = m. \end{cases} \tag{4.33}$$

4.3.3 Diversity Order Analysis

The diversity order of the proposed SISO wireless system assisted by MIRS panels can be obtained as

$$d = \lim_{\gamma_0 \to \infty} \frac{-\log P_{\text{out}}^{\infty}}{\log \gamma_0}. \tag{4.34}$$

After substituting (4.33) into (4.34) and performing simplification, the result is

$$d = \begin{cases} \sum_{l=1}^{L} \sum_{i=1}^{N_l} \min\{m_{\alpha_{li}}, m_{\beta_{li}}\}; & m_{\alpha_{li}} \neq m_{\beta_{li}} \\ \\ m \sum_{l=1}^{L} N_l; & m_{\alpha_{li}} = m_{\beta_{li}} = m \end{cases} \tag{4.35}$$

Remark 4.1. The diversity order depends on the minimum fading parameter (m) between the transmitter-IRS panel and IRS panel-receiver links, the number of IRS elements in each panel, and the number of IRS panels. To the best of the authors' knowledge, it is a novel diversity order expression.

4.4 Results and Discussion

In this section, we perform numerical analysis and simulations to analyze the IRS panels assisted SISO communication system using the derived OP expressions. To validate our derived OP expression, we also present Monte Carlo simulations. For presentation, we make the following assumptions regarding the parameters: $m_{\alpha_l} = m_1, m_{\beta_l} = m_2, d_{\alpha_l} = d_1, d_{\beta_l} = d_2, \delta_{\alpha_l} = \delta_1, \delta_{\beta_l} = \delta_2, \Omega_{\alpha_l} = d_{\alpha_l}^{-\delta_{\alpha_l}} = \Omega_1 = d_1^{-\delta_1}, \Omega_{\beta_l} = d_{\beta_l}^{-\delta_{\beta_l}} = \Omega_2 = d_2^{-\delta_2}, \forall l$. Additionally, unless specified otherwise, the following set of parameters are used for the numerical and simulation results. We consider a sub-6G scenario similar to [35], with a system bandwidth of 180 KHz and a noise power spectral density of -173 dBm/Hz. The distances (in meters) are set as $d_1 = d_2 = 150$ m, and the path loss exponents are $\delta_1 = \delta_2 = 2$. The Nakagami fading parameter is $m_1 = m_2$[2], and the reference path loss at the reference distance $d_0 = 1$ m is -30 dB. The threshold SNR is $\gamma_{th} = 10$ dB, and the number of IRS panels is $L = 2$. Each figure depicts the OP performance as a function of the transmitted power P (dBm).

[2] m_1 and m_2 denote the Tx-IRS and IRS-Rx links fading parameters, respectively.

Figure 4.2 depicts the OP by varying P and N. We employ both CLT and LSE analytical approaches to demonstrate their precision. In Figure 4.2, it becomes clear that for small values of N, the CLT-based approximation method lacks accuracy. However, for larger values of N, the CLT closely matches the simulation results, similar to the accuracy observed with the LSE approach in both Figure 4.2 and Figure 4.3.

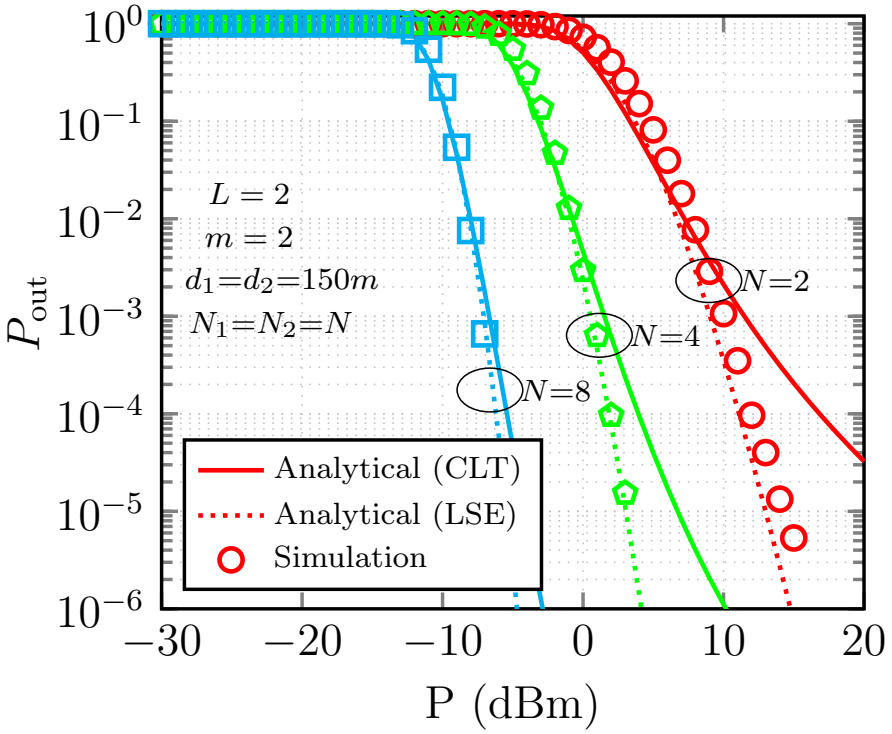

FIGURE 4.2: OP performance with varying N and a fixed $L = 2$.

Figure 4.3 shows change in performance due to the shaping parameter, m, in the Nakagami-m fading channel. The OP performance is observed to improve with an increase in m, as it implies a decrease in the severity of fading. Remarkably, we observe that the SNR gain exhibits a more substantial increase when m transitions from 0.5 to 1 compared to the increments from 1 to 3, or 3 to 5. This suggests that raising m beyond a certain threshold may not yield a notably greater improvement in SNR gain.

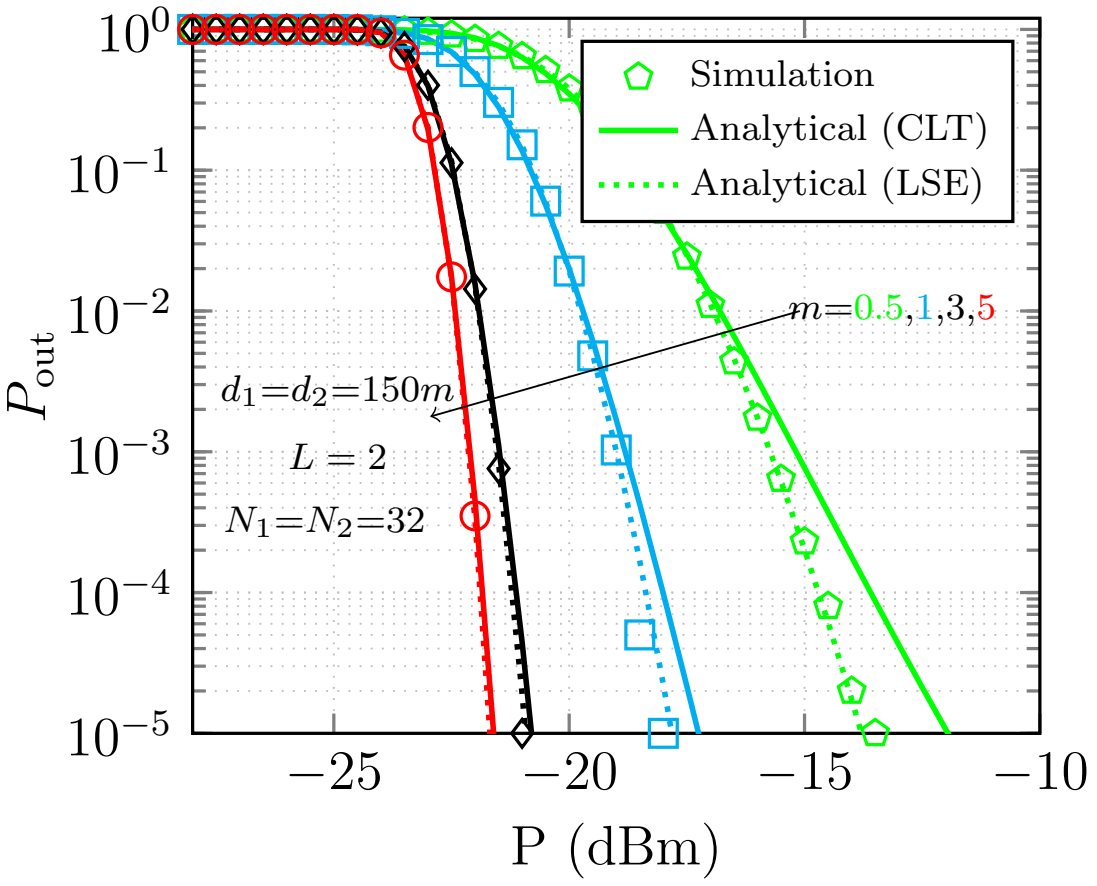

FIGURE 4.3: OP vs. P with varying the fading parameter m.

Figure 4.4 shows the impact of L on the OP performance. As L increases, the enhancement in OP performance becomes evident, primarily attributed to the augmented diversity order. For instance, at $P_{\text{out}} = 10^{-3}$, increasing L from 1 to 4 results in a performance enhancement of approximately 1 dB in terms of transmit power. Further, Figure 4.5 verifies the precision of our asymptotic OP expression in high SNR conditions. Noticeably, the asymptotic OP converges toward the simulation results, affirming the reliability of P_{out}^{∞}.

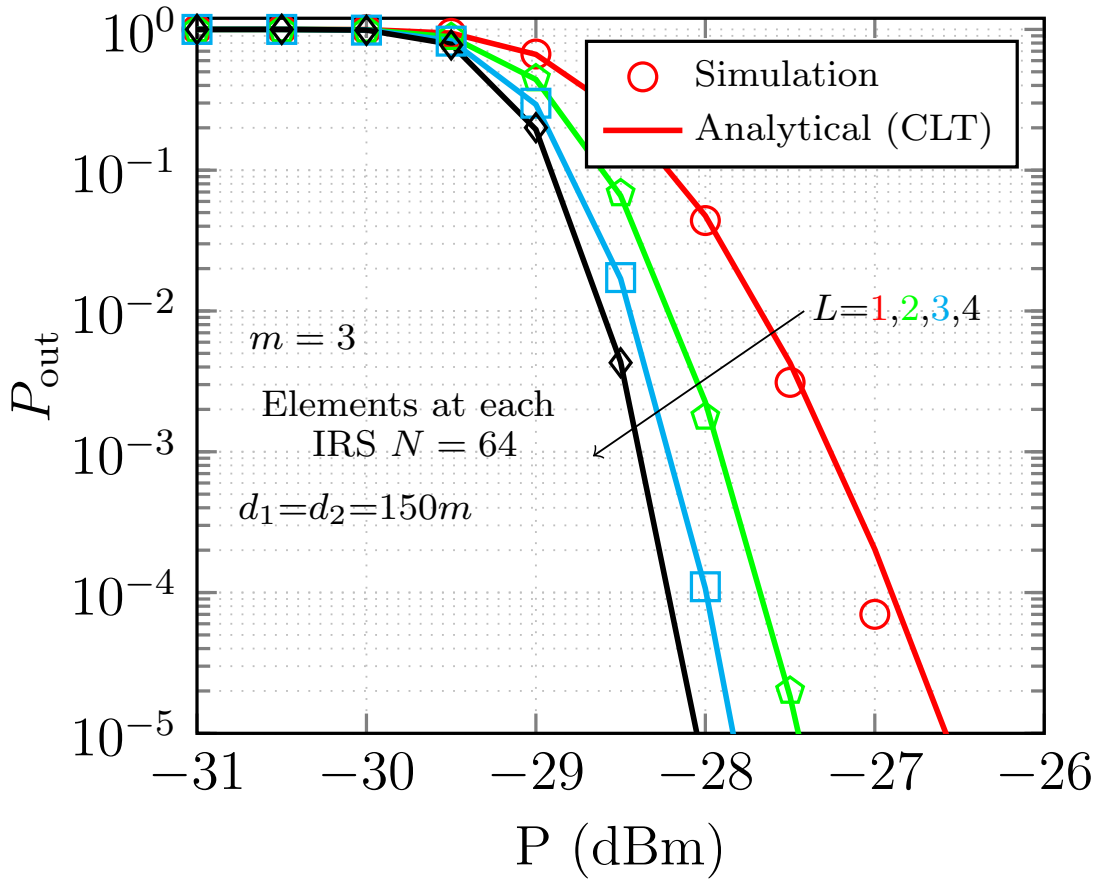

FIGURE 4.4: OP vs. P with varying IRS Panels (L)

4.5 Summary

We have conducted an extensive analysis of SISO communication systems employing MIRS panels over i.n.d. Nakagami-m fading channels. We have derived accurate OP expressions by employing CLT and LSE approaches. Furthermore, we have also obtained a new asymptotic OP. A closed-form diversity order expression is derived, which is found to be dependent on the minimum fading parameter between the transmitter-IRS panel and IRS panel-receiver links, as well as the number of IRS panels. To verify the accuracy of the theoretical analysis, Monte Carlo simulations have been conducted, yielding results consistent with the presented analysis. We have examined how system parameters, including the fading parameter (m) and the

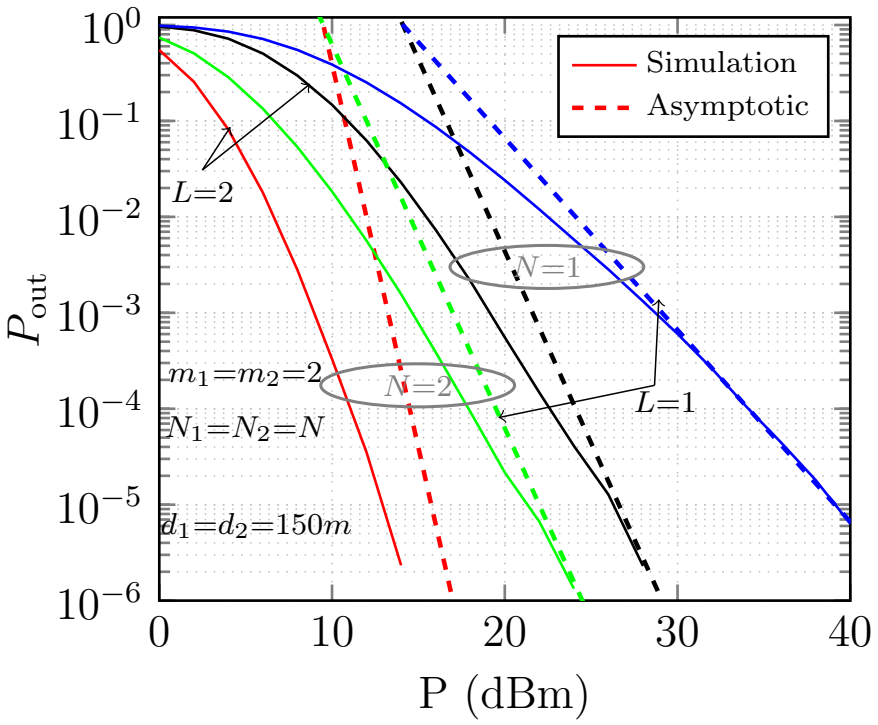

FIGURE 4.5: OP vs. P with varying both L and N_l

number of IRS panels, influence the system's OP performance. Results show that IRS panel selection and fading parameters significantly affect system performance, apart from the number of IRS elements.